DEVELOPMENTAL BIOLOGY

Recycling of parental histones preserves the epigenetic landscape during embryonic development

Dominik Mühlen[1,2]†, Xiaojuan Li[1]†, Oleksandr Dovgusha[1]†, Herbert Jäckle[2], Ufuk Günesdogan[1,2]*

Epigenetic inheritance during DNA replication requires an orchestrated assembly of nucleosomes from parental and newly synthesized histones. We analyzed *Drosophila His^C* mutant embryos harboring a deletion of all canonical histone genes, in which nucleosome assembly relies on parental histones from cell cycle 14 onward. Lack of new histone synthesis leads to more accessible chromatin and reduced nucleosome occupancy, since only parental histones are available. This leads to up-regulated and spurious transcription, whereas the control of the developmental transcriptional program is partially maintained. The genomic positions of modified parental histone H2A, H2B, and H3 are largely restored during DNA replication. However, parental histones with active marks become more dispersed within gene bodies, which is linked to transcription. Together, the results suggest that parental histones are recycled to preserve the epigenetic landscape during DNA replication in vivo.

INTRODUCTION

Eukaryotic chromatin is packaged into nucleosomes, which consist of DNA wrapped around a histone octamer (two copies of each of H2A, H2B, H3, and H4) as well as linker DNA and the linker histone H1. Histones are decorated with multiple posttranslational modifications (PTMs), which play an integral part in the epigenetic transmission of chromatin structure and transcriptional regulation across cell generations.

During replication of DNA in S phase of the cell cycle, replication fork progression evicts transcription factors and nucleosomes, and the nascent DNA undergoes maturation by reestablishing chromatin accessibility (*1*, *2*). Parental, preexisting nucleosomes distribute semiconservatively onto each new DNA strand after replication (*3*, *4*). Specifically, H3-H4 tetramers and H2A-H2B dimers are recycled and reassembled together with new histones, whose expression is replication coupled, to form nucleosomes behind the replication fork (fig. S1A) (*5*). Recycled histones maintain their PTMs, which can serve as a "template" to reestablish the epigenetic and transcriptional landscape after DNA replication (*6*, *7*). This model implies that parental histones harbor a "memory" of their genomic position before passage of the replication fork (*8*). Notably, bulk analyses of histone populations in yeast and HeLa cells show that nucleosomes are restored at the same positions after DNA replication (*9*, *10*). A study of tagged parental histone H3 before and after replication in mouse embryonic stem cells (ESCs) revealed local recycling of parental nucleosomes at repressed chromatin domains as compared to random dispersal of parental nucleosomes within active domains (*11*).

How parental nucleosomes are relocated during embryonic DNA replication remains unknown. To address this question, we leveraged the *Drosophila melanogaster* mutant *His^C*, which carries a chromosomal deletion including all canonical histone genes (*His1*, *His2A*, *His2B*, *His3*, and *His4*) (*12*). Homozygous *His^C*

mutant embryos have a late embryonic lethal phenotype. The maternal pool of histone mRNA supports the first 14 cell cycles (*12*, *13*), but after the maternal-to-zygotic transition, *His^C* mutant embryos lacked histone transcripts in S phase 15 (S_{15}) (Fig. 1A), consistent with our previous study (*12*). This leads to prolonged DNA replication and results in a cell cycle arrest in $G2_{15}$ (fig. S1, B and C) (*12*, *14*). Thus, nucleosome assembly relies on parental nucleosomes without additional supply of newly synthesized histones during DNA replication in S_{15} of *His^C* mutant embryos (fig. S1A). We made use of *His^C* mutant embryos as a model system to study nucleosome assembly in a developing embryo. Our data suggest that parental histones harboring PTMs are recycled, and their genomic positions are restored during DNA replication to preserve the epigenetic landscape.

RESULTS

Reassembly of chromatin in the absence of histone synthesis

To determine how a lack of newly synthesized histones affects chromatin maturation, we performed ATAC-seq (assay for transposase-accessible chromatin using sequencing) with embryos at 3.5 to 4, 4.5 to 5, 5.5 to 6, and 6.5 to 7 hours after egg laying (AEL) (fig. S2A), covering progression through S_{15}-S_{16} in wild-type and S_{15}-$G2_{15}$ arrest in *His^C* mutant embryos (fig. S1C) (*12*). The principal components analysis (PCA) of the ATAC-seq data showed global differences in chromatin accessibility between the two genotypes along PC1 (68%) (fig. S2B). However, PC2 separated wild-type but not *His^C* mutant samples based on developmental age (11%). These data suggest that the global chromatin accessibility pattern changes during S_{15}-S_{16} in wild-type embryos but less so during the prolonged S_{15} and $G2_{15}$ arrest of *His^C* mutant embryos.

Fragment size distribution showed that *His^C* and wild-type embryos were enriched for nucleosome-depleted regions [NDRs; ≤120 base pairs (bp)] (fig. S2C). However, the typical periodicity of nucleosome-spanning fragments [>120 bp] was lower in *His^C* mutant embryos as compared to wild-type at all stages examined, with the smallest median fragment size at 6.5 to 7 hours AEL. To further analyze the distribution of these fragments, we mapped

[1]University of Göttingen, Göttingen Center for Molecular Biosciences, Department of Developmental Biology, Justus-von-Liebig-Weg 11, 37077 Göttingen, Germany. [2]Max Planck Institute for Multidisciplinary Sciences, Department for Molecular Developmental Biology, Am Fassberg 11, 37077 Göttingen, Germany.
†These authors contributed equally to this work.
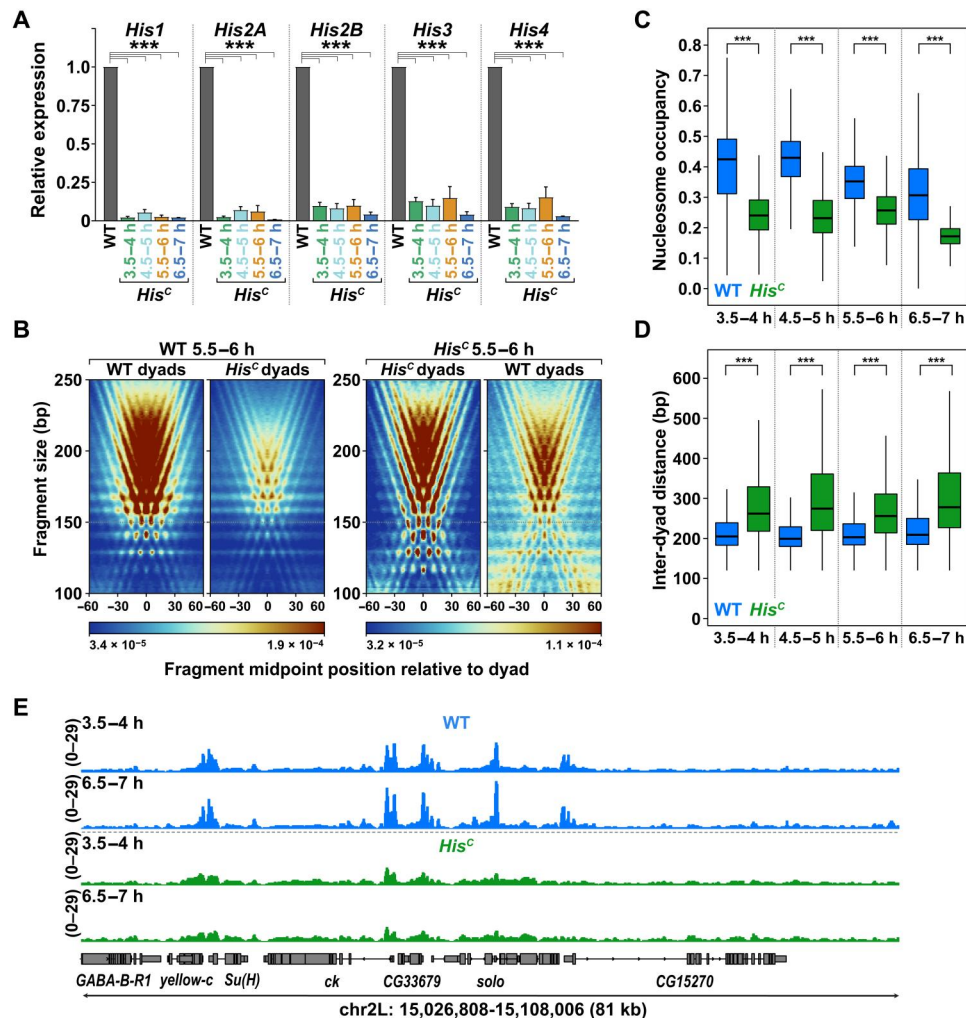*Corresponding author. Email: ufuk.guenesdogan@uni-goettingen.de

Fig. 1. Nascent chromatin in *His^C* mutants does not undergo maturation. (**A**) Quantitative polymerase chain reaction (qPCR) for histone genes *His1*, *His2A*, *His2B*, *His3*, and *His4* with cDNA from wild-type (WT) or *His^C* mutant embryos at indicated hours (h) after egg laying (AEL). $\Delta\Delta Ct$ ±SD; normalization using *act5c* (housekeeping gene) and matched WT embryos as a reference (= 1); $n = 5$ biological replicates; two-sided, unpaired Student's *t* test, ***$P < 0.0001$. (**B**) V plots show density of nucleosome-spanning fragments [>120 base pairs (bp)] and sizes relative to nucleosome dyad centers of WT or *His^C* mutant embryos. ATAC-seq (assay for transposase-accessible chromatin using sequencing) data from embryos at 5.5 to 6 hours AEL. (**C**) Median nucleosome occupancy ±2 kb of transcription start sites (TSSs). ATAC-seq data from embryos at 3.5 to 4, 4.5 to 5, 5.5 to 6, and 6.5 to 7 hours AEL. Unpaired Wilcoxon test, ***$P < 0.0001$. (**D**) Median inter-dyad distances ±2 kb of TSSs. ATAC-seq data from embryos at 3.5 to 4, 4.5 to 5, 5.5 to 6, and 6.5 to 7 hours AEL. Unpaired Wilcoxon test, ***$P < 0.0001$. (**E**) Representative snapshots of ATAC-seq coverage tracks. Biological replicates are merged. chr, chromosome.

the density of their midpoints and sizes relative to the nucleosome dyad centers (*15*, *16*). Wild-type and *His^C* mutant embryos at all stages showed a characteristic V-shaped horizontal and vertical periodicity of nucleosome-spanning fragments at and around the dyad centers (Fig. 1B and fig. S2D), as described previously (*16*). However, most fragments were smaller in *His^C* mutant (~120 to 145 bp) as compared to wild-type (~155 to 180 bp) embryos. This difference was particularly evident when we mapped nucleosome-spanning fragments of *His^C* mutant embryos at nucleosome dyad centers of wild-type (Fig. 1B). This suggests the presence of subnucleosomes, which are wrapped by shorter stretches of DNA than complete nucleosomes (*17*). Overall, *His^C* mutant embryos showed a reduction in the median nucleosome occupancy levels at transcription start sites (TSSs) ±2 kb and putative regulatory elements as well as an increase in the median distance between

nucleosome dyad centers (Fig. 1, C and D, and fig. S2, E and F). These data suggest that, in the absence of newly synthesized histones, parental histones are recycled but reassembled at a lower occupancy and some potentially as subnucleosomes.

Next, we inspected ATAC-seq coverage tracks, which showed that *His^C* mutant embryos have reduced but detectable peaks that overlap with wild-type peaks (Fig. 1E and fig. S3A). This finding suggests that nucleosomes are more disorganized in *His^C* mutants, and their NDRs are less defined. In addition, large fraction of ATAC-seq reads from wild-type was mapped to a small proportion of the genome, indicating localized enrichment (fig. S3B). In contrast, ATAC-seq reads from *His^C* mutant embryos showed a more uniform distribution across the genome, which indicates an overall increase in chromatin accessibility. This finding prompted us to analyze nucleosomal arrays around TSSs. ATAC-seq signals

showed a characteristic positioning of nucleosomes in wild-type embryos: The NDRs corresponded to TSSs and were surrounded by a −1 nucleosome upstream and a well-positioned +1 nucleosome downstream, followed by regularly phased +2 and +3 nucleosomes (Fig. 2A and fig. S4). In *His*^C mutant embryos, the −1/+1 nucleosomes were well positioned but reduced; the +2/+3 nucleosomes were also reduced but showed a positional shift and a gain in signal between the nucleosomes (Fig. 2A and fig. S4). This was particularly evident at the TSSs of highly expressed genes, which we identified by RNA sequencing (RNA-seq) (see below). In addition, we analyzed fragment length distribution at TSSs ±600 bp by density plots. They revealed an enrichment of nucleosomal fragments in regular arrays up- and downstream of TSSs in wild-type (Fig. 2B and fig. S5). In contrast, *His*^C mutant embryos exhibit an enrichment and broad distribution of nucleosomal and subnucleosomal fragments downstream of TSSs, which is pronounced downstream of the +1 nucleosome of highly expressed genes.

Thus, although the recycled parental nucleosomes were well positioned around TSSs in S_{15}/$G2_{15}$ of *His*^C mutant embryos, their levels were reduced, and they were not regularly phased in nucleosomal arrays further downstream of TSSs. Furthermore, it appears that the displacement of nucleosomes during transcription (*18*) results in an increased reassembly of subnucleosomes. We infer that the characteristic nucleosomal landscape is partially

reestablished and more disorganized after S_{15} in *His*^C mutant embryos, resembling profiles of nascent chromatin shortly after DNA replication in both *Drosophila* S2 cells and ESCs (*1*, *2*).

Recycling and deposition of parental linker histone H1

The formation of nucleosome arrays and chromatin compaction also depend on linker histone H1 (*19*, *20*). In HeLa cells, most histone H1 variants are incorporated into chromatin only after its maturation (*21*). *Drosophila* harbors only a single somatic histone H1 isoform, which is expressed together with the other canonical histones during S phase of cell cycle (*12*, *22*). To determine whether the lack of new histone H1 affects its distribution, we performed CUT&Tag (cleavage under targets and tagmentation) (*23*) for H1 with embryos at 5.5 to 6 hours AEL (fig. S6), when most cells have completed or proceeded through late S_{15} in *His*^C mutants (fig. S1C) (*12*). Coverage tracks showed that the distribution of H1 was comparable in wild-type and *His*^C mutant embryos (Fig. 3A). H1 contacts the nucleosomal dyad and both linker DNAs of one nucleosome (*20*, *24*). H1 was enriched around nucleosome borders and slightly enriched at the midpoint of nucleosomes in wild-type (Fig. 3B). This was also the case in *His*^C mutant embryos but at reduced levels, consistent with reduced nucleosome occupancy (Fig. 1C and fig. S2E). Notably, median H1 fragment lengths corresponded to those of mononucleosomal DNA and linker DNAs
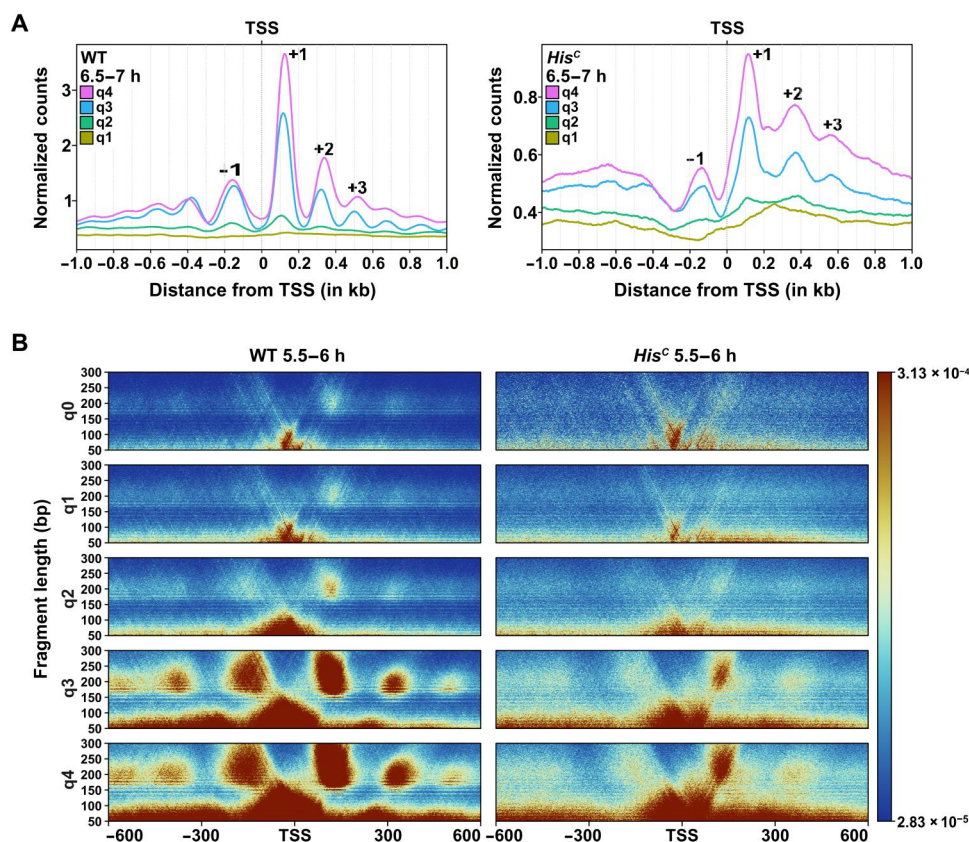
Fig. 2. Disorganized nucleosomal arrays in *His*^C mutants. (**A**) Normalized ATAC-seq count distribution of mononucleosomal reads (180 to 240 bp) at TSSs ±1 kb of WT (left) and *His*^C mutant (right) embryos at 6.5 to 7 hours AEL. ATAC-seq reads were divided on the basis of corresponding gene expression quartiles as determined by RNA sequencing (RNA-seq) (q1 = lowest). Note the different scales for data with WT or *His*^C mutant embryos. (**B**) Density plot showing ATAC-seq fragment size distribution and enrichment at TSSs ±600 bp of WT (left) and *His*^C mutant (right) embryos at 5.5 to 6 hours AEL. ATAC-seq reads were divided on the basis of corresponding gene expression quartiles as determined by RNA-seq (q0 = no reads and q1 = lowest).
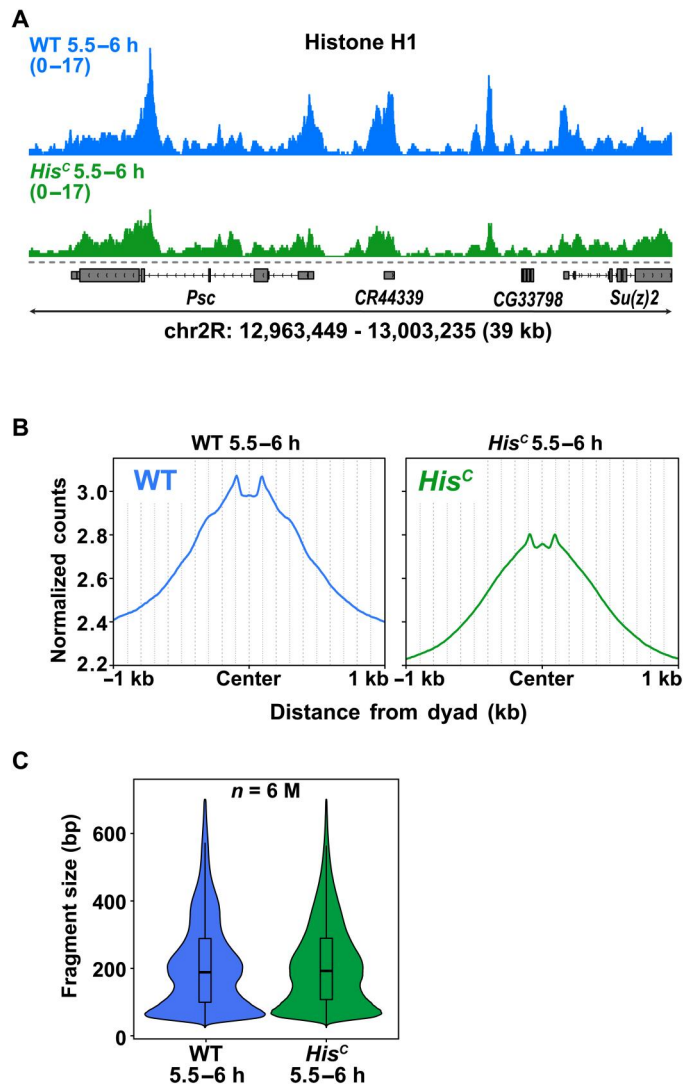
Fig. 3. Histone H1 is recycled in *His^C* mutant embryos. (**A**) Representative snapshot of histone H1 CUT&Tag (cleavage under targets and tagmentation) coverage tracks of WT (blue) and *His^C* mutant (green) embryos at 5.5 to 6 hours AEL on chr 2L. Biological replicates are merged. (**B**) Profile plot of histone H1 CUT&Tag–normalized counts at nucleosome dyad centers of WT (blue) or *His^C* mutant (green) embryos at 5.5 to 6 hours AEL. (**C**) Fragment size distribution of histone H1 CUT&Tag data with WT (blue) and *His^C* mutant (green) embryos at 5.5 to 6 hours AEL. *n* = number of fragments in million (M).

(~200 bp) (Fig. 3C). Thus, despite the lack of zygotic histone H1 expression in *His^C* mutants, parental histone H1 is recycled and appropriately deposited during and/or after DNA replication.

Up-regulation of transcription in *His^C* mutant embryos

Chromatin accessibility enables binding of transcription factors to regulatory elements. Our results indicate that the chromatin is overall more accessible in *His^C* mutant embryos, so we hypothesized that transcription is up-regulated relative to wild-type. To test this, we examined transcript levels by RNA-seq of embryos at 3.5 to 4, 4.5 to 5, 5.5 to 6, and 6.5 to 7 hours AEL. Similar to the ATAC-seq data, PCA separated samples based on genotype (PC1, 68%) (fig. S7A).

However, PC2 also separated both wild-type and *His^C* mutant samples based on developmental age (PC2, 18%), suggesting that *His^C* mutant embryos partially proceed with the developmental program, consistent with our earlier study (*12*). We clustered genes based on their expression dynamics. This revealed two main clusters with either up- or down-regulated genes along the four developmental time points of wild-type and *His^C* mutant embryos, respectively (Fig. 4A and fig. S7B). Notably, the expression profile of these two clusters was different at 4.5 to 5 hours AEL in *His^C* mutant embryos as compared to wild-type, which is likely due to the slow progression of DNA replication that interferes with transcription (*14, 25*). Moreover, Gene Ontology (GO) analysis for the main cluster of up-regulated genes in both genotypes revealed significantly enriched terms associated with developmental processes such as *cell migration*, *cell part morphogenesis*, and *imaginal disc morphogenesis* (fig. S7C). In contrast, the main cluster of down-regulated genes is largely linked to "general" cellular processes such as *RNA splicing* or *DNA metabolic process* in both genotypes (fig. S7D).

Consistent with our hypothesis, differential gene expression analysis identified a large number of genes that were significantly up-regulated in *His^C* mutant compared to wild-type embryos [e.g., 2944 at 6.5 to 7 hours AEL, an absolute $\log_2$ fold change of >1, and an adjusted P value (P_{adj}) of <0.01] (Fig. 4B and fig. S8A). These included a small subset of genes associated with spermatogenesis such as *always early*, *wurstfest*, and *cookie monster* that are normally not expressed during wild-type embryogenesis (Fig. 4C and fig. S8B). Thus, we asked whether genes within repressed chromatin are globally derepressed in *His^C* mutant embryos. We used published chromatin immunoprecipitation sequencing data from wild-type embryos at 4 to 8 hours AEL to map silenced genes, which are enriched for the heterochromatin-associated mark H3K9me3 (*26*). Expression analysis showed that these genes were up-regulated in *His^C* mutant embryos, but the median levels remained relatively low [$\log_2$(normalized counts + 1) < 2] (fig. S8C). In addition, when we assigned significantly up-regulated genes in *His^C* mutant embryos to the corresponding expression levels in wild-type (q0 = no reads and q1 to q4 = expression quartiles), we found that the majority of up-regulated genes (>60%) in *His^C* mutant embryos belong to the lowly (q1) and moderately (q2) expressed genes in wild-type embryos at the same stage (Fig. 4D).

Together, these findings suggest that, although *His^C* mutant embryos can partially control the transcriptional program associated with development, the lack of histone synthesis leads to ectopic expression of some normally inactive genes and increased expression of genes, which are lowly and moderately expressed in wild-type embryos. Notably, despite the transcriptional activity of *His^C* mutant embryos and the role of the transcriptional machinery in the maturation of nascent chromatin after DNA replication (*1, 2*), the global nucleosomal landscape is not fully reestablished, which is likely due to reduced nucleosome occupancy.

Spurious transcription initiation in *His^C* mutant embryos

To gain mechanistic insight into how the lack of histone synthesis and nucleosome occupancy up-regulates transcription, we performed CUT&Tag with embryos 4.5 to 5 hours and/or 5.5 to 6 hours AEL to map total RNA polymerase II (RNAPII); serine-2-phosphorylated RNAPII (RNAPIIS2P), which is associated with the transition from pausing to elongation (*27*); and the

Fig. 4. Up-regulation of transcriptional activity in *His^C* mutant embryos. (**A**) Clustering of genes based on their RNA-seq expression dynamics of WT (blue) or *His^C* mutant (green) embryos at 3.5 to 4, 4.5 to 5, 5.5 to 6, and 6.5 to 7 hours AEL . Shown are the two major clusters of up- or down-regulated genes. Numbers of genes in each cluster are indicated. (**B**) MA plots showing differential gene expression analysis of RNA-seq data with WT and *His^C* mutant embryos at 3.5 to 4 and 6.5 to 7 hours AEL. Each transcript is represented by a dot (gray: not significant, red: significantly up-regulated, blue: significantly down-regulated; significance threshold: absolute $\log_2$fold change of >1 and P_{adj} of <0.01; number of differentially expressed genes is indicated). (**C**) Heatmap of RNA-seq expression values (*z* score) of spermatogenesis-related genes, which are significantly up-regulated in *His^C* mutants. (**D**) Bar plot shows the number (in %) of differentially up-regulated genes in *His^C* mutants at 3.5 to 4, 4.5 to 5, 5.5 to 6, and 6.5 to 7 hours AEL in corresponding WT expression quartiles (q0 = no reads and q1 = lowest). (**E**) Profile plots of serine-2-phosphorylated RNAPII (RNAPIIS2P) CUT&Tag-normalized counts across gene bodies of WT (left) and *His^C* mutant embryos (right) at 4.5 to 5 or 5.5 to 6 hours AEL separated by associated gene expression quartiles (q1 = lowest). Note the different scales for data with WT or *His^C* mutant embryos. TES, transcription end site. (**F**) Profile plots of H3K36me3 CUT&Tag-normalized counts across gene bodies of WT (blue) and *His^C* mutant (green) embryos at 4.5 to 5 or 5.5 to 6 hours AEL.

transcription elongation-coupled histone mark H3K36me3 (fig. S9, A to C) (28). In wild-type embryos, total RNAPII was enriched at TSSs and throughout the gene body (fig. S9D). Both RNAPIIS2P and H3K36me3 showed a promoter-proximal peak and increasing enrichment in 5′ to 3′ direction of actively transcribed gene bodies (Fig. 4, E and F, and fig. S9, E and F). In contrast, RNAPII and RNAPIIS2P were reduced at TSSs but still enriched in gene bodies of His^C mutant embryos (Fig. 4E and fig. S9, D and E). Similarly, promoter-proximal H3K36me3 was depleted but was enriched toward the 3′ end of gene bodies (Fig. 4F and fig. S9, E and F). These results suggest that the lack of histone synthesis in His^C mutant embryos leads to premature release of paused RNAPII into transcriptional elongation and/or initiation of spurious transcription within gene bodies.

To address whether pausing of RNAPII is impaired in His^C mutant embryos, we analyzed H3K4me2 enrichment at 4.5 to 5 and 5.5 to 6 hours AEL. H3K4me2 is enriched on nucleosomes flanking NDRs and associated with RNAPII stalling at TSSs, and thus it is coupled to the onset of transcription (23). We performed CUTAC (cleavage under targeted accessible chromatin) (29) for H3K4me2 (fig. S10A), which targets transcription-coupled, accessible regulatory sites. H3K4me2 CUTAC peaks overlapped with ATAC-seq peaks genome wide and at TSSs in wild-type (Fig. 5A and fig. S10, B to D). Similarly, enrichment of H3K4me2 CUTAC and ATAC-seq correlated well genome wide in His^C mutants (fig. S10, C and D). However, H3K4me2 CUTAC coverage was broadly enriched downstream of TSSs (Fig. 5A and fig. S10B). This shows that H3K4me2-modified nucleosomes are enriched within gene bodies of His^C mutant embryos, suggesting a premature release of RNAPII into elongation.

Next, we examined whether the lack of histone synthesis and diminished nucleosome occupancy are associated with spurious transcription. We mapped transcription start regions (TSRs) by STRIPE-seq (survey of transcription initiation at promoter elements with high-throughput sequencing) (30) using embryos at 5.5 to 6 and 6.5 to 7 hours AEL. STRIPE-seq counts at promoter regions positively correlated with transcript levels, consistent with elevated transcription (fig. S11A). The density of TSRs was centered around TSS positions but less pronounced in His^C mutant embryos as compared to wild-type (fig. S11B). Consistently, TSRs were largely annotated to promoter regions (≥75% in wild-type and ≥55% in His^C mutant), but in His^C mutants, a considerably larger fraction of TSRs was associated with other genomic regions, including exons, introns, and intergenic regions (≤20% in wild-type and ≤39% in His^C mutants) (Fig. 5B and fig. S11, C and D). This difference became more evident when we called differential TSRs in His^C mutants, many of which were associated with regions outside of promoters (~55%) (Fig. 5C). Consistent with the TSR annotation, we found a significant increase of normalized STRIPE-seq read counts at exons and introns (Fig. 5D). To further test whether intergenic TSRs correlate with spurious transcription, we analyzed normalized RNA-seq counts 1 kb downstream of these TSRs and found a significant increase in His^C mutants (Fig. 5, B and E, and fig. S11D). Together, these findings suggest that reduced nucleosome occupancy and the lack of histone synthesis in His^C mutants cause spurious transcription initiation within gene bodies and intergenic regions.

Genomic positioning of modified parental nucleosomes during DNA replication

PTMs are associated with chromatin accessibility and transcriptional control. Given that His^C mutants can at least partially control the developmental transcriptional program, we asked whether the epigenetic landscape is reestablished during and/or after S_{15} by performing CUT&Tag for H3K4me3 at 3.5 to 4, 5.5 to 6, and 6.5 to 7 hours AEL (fig. S12, A and B). H3K4me3 deposition is transcription coupled and represents a hallmark of active transcription (23). Wild-type embryos showed a bimodal enrichment of H3K4me3 at TSSs, followed by a decline across gene bodies, and the level of enrichment correlated positively with transcript abundance quartiles (Fig. 6A and fig. S12C). In His^C mutants, H3K4me3 was still enriched at TSSs, but the levels were reduced and followed by a broader profile across gene bodies (Fig. 6A and fig. S12C), which is consistent with spurious transcription initiation. Furthermore, coverage tracks showed a similar H3K4me3 enrichment pattern but reduced levels in His^C mutant as compared to wild-type embryos (Fig. 6B and fig. S13A).

To compare H3K4me3-enriched loci, we used narrow peak calling [Model-based Analysis of ChIP-seq 2 (MACS2)]. This comparison showed a subset of common H3K4me3 peaks with lower levels in His^C mutant as compared to wild-type embryos (Fig. 6, B and C, and fig. S13, A to C). In addition, we identified a subset of peaks predominantly within gene bodies with low but significant levels of H3K4me3 specific for His^C mutants (Fig. 6C and fig. S13, B and C). Considering that H3K4me3 enrichment profiles did not significantly change across developmental time points (Fig. 6B and fig. S13), these results suggest that parental histones with H3K4me3 might be deposited in close proximity or are located even at the genomic position that they were holding before replication, while their dispersal across gene bodies could be a consequence of transcription. Alternatively, unmodified parental histones could be sufficient to reestablish the H3K4me3 landscape as a result of transcriptional activity.

To distinguish between these possibilities, we performed CUT&Tag for the transcription-independent marks H3K27ac and H3K27me3 at 4.5 to 5 and 5.5 to 6 hours AEL. H3K27ac is associated with active promoters and enhancers (31), displayed a bimodal enrichment at TSSs, and is relatively depleted toward the 3′ end of gene bodies in wild-type embryos (Fig. 7A and fig. S14, A and B). The bimodal enrichment of H3K27ac at TSSs was reduced in His^C mutant compared to wild-type embryos, and H3K27ac was enriched throughout the gene bodies (Fig. 7A and fig. S14B). Narrow peak calling again showed a robust subset of peaks common to both wild-type and His^C mutant embryos in addition to genotype-specific peaks (Fig. 7B and fig. S14C). Inspection of coverage tracks revealed a similar enrichment of H3K27ac at many loci in wild-type and His^C mutant embryos (Fig. 7C and fig. S14D). However, the enrichment profiles were typically broader in His^C mutant embryos, and some regions showed ectopic enrichment (Fig. 7C and fig. S14D). The analysis of H3K27ac peaks in intergenic regions showed a comparable enrichment profile but at different levels in both genotypes (Fig. 7D and fig. S14E). Thus, the pattern of H3K27ac enrichment is similar, particularly, at intergenic regions in both His^C mutant and wild-type embryos, while differences of H3K27ac enrichment within gene bodies are likely due to transcriptional activity, consistent with the dispersal of H3K4me3.
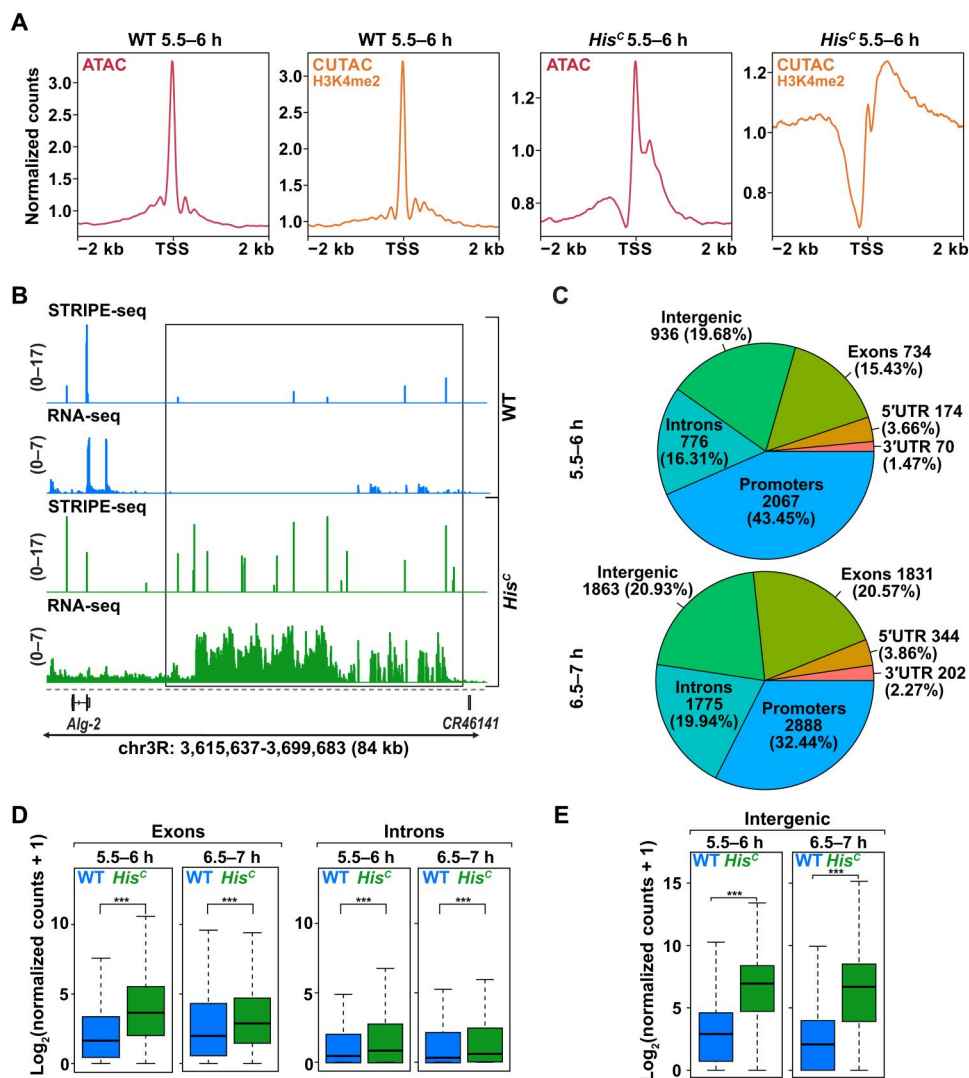
Fig. 5. Premature release of RNAPII into elongation and spurious transcription initiation in *His^C* mutant embryos. (**A**) Comparison of ATAC-seq (≤120-bp reads, red) and H3K4me2 CUTAC (≤120-bp reads, orange) profile plots of WT and *His^C* mutant embryos at 5.5 to 6 hours AEL at TSSs ±2 kb. Note the different scales for data with WT or *His^C* mutant embryos. (**B**) Representative snapshot of STRIPE-seq (survey of transcription initiation at promoter elements with high-throughput sequencing) and RNA-seq coverage tracks of WT (blue) and *His^C* mutant (green) embryos at 6.5 to 7 hours AEL on chr 3R. (**C**) Genomic annotation of differential TSRs (*His^C* versus WT) at 5.5 to 6 and 6.5 to 7 hours AEL. 5′UTR, 5′ untranslated region. (**D**) Box plots showing normalized STRIPE-seq counts within exons and introns of WT (blue) and *His^C* mutant (green) embryos at 5.5 to 6 and 6.5 to 7 hours AEL. Unpaired Wilcoxon t test, ***$P < 0.0001$. (**E**) Box plots showing normalized RNA-seq counts 1 kb downstream of intergenic TSRs of WT (blue) and *His^C* mutant (green) embryos at 5.5 to 6 and 6.5 to 7 hours AEL. Unpaired Wilcoxon t test, ***$P < 0.0001$.

The polycomb repressive complex 2–dependent mark H3K27me3 is associated with repression. As for H3K4me3 and H3K27ac, the levels of H3K27me3 enrichment were reduced in *His^C* mutant embryos, but both wild-type and *His^C* mutant embryos exhibited overlapping broad H3K27me3-enriched domains (Fig. 7, E and F, and fig. S15, A to C). Notably, we also called peaks specific for each genotype, which, however, showed very low levels of H3K27me3 enrichment in both genotypes (Fig. 7F and fig. S15B). Together, these data suggest that parental histone H3 carrying active or repressive marks largely preserve their genomic position during and after replication in embryos, while dispersal of nucleosomes within gene bodies containing histones with active marks correlates with transcription.

Last, we asked whether H2A-H2B dimers decorated with PTMs are recycled in a similar manner as H3-H4 tetramers. We performed CUT&Tag for H2AK9ac and H2BK16ac at 4.5 to 5 and 5.5 to 6 hours AEL (figs. S6 and S16) and found that both modifications were broadly enriched across gene bodies in both genotypes (fig. S17A). Similar to the H3 modifications, peak calling shows a robust subset of common peaks for H2AK9ac and H2BK16ac in both wild-type and *His^C* mutant embryos as well as genotype-specific peaks (Fig. 8, A to D, and fig. S17, B and C). The levels of these modifications were reduced at 4.5 to 5 hours as compared to 5.5 to 6 hours AEL in *His^C* mutant embryos, suggesting de novo acetylation of unmodified nucleosomes over developmental time. Similar to H3K4me3 and H3K27ac, analysis of H2AK9ac and H2BK16ac
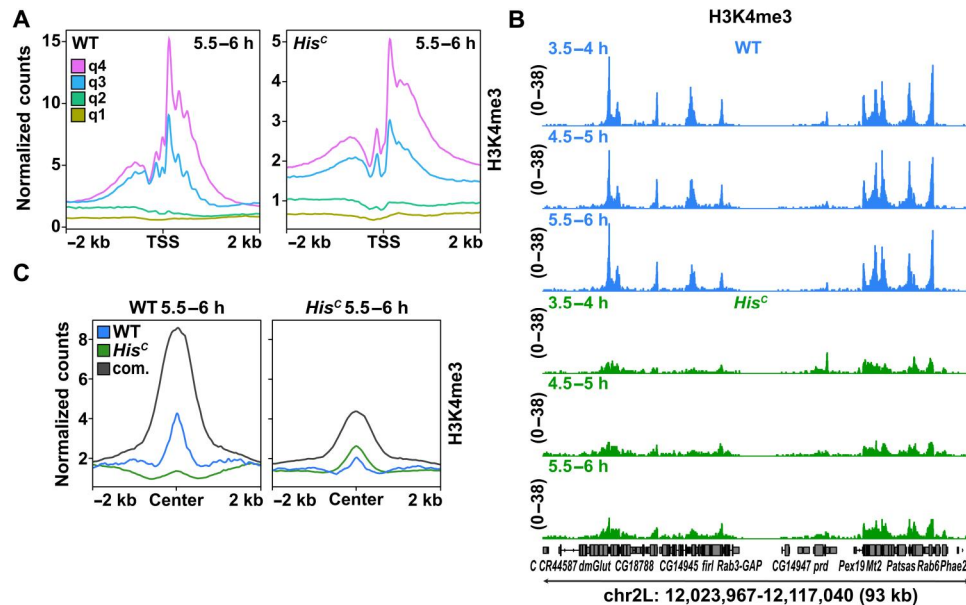
Fig. 6. Genomic positions of H3K4me3 are largely preserved in *His^C* mutant embryos. (**A**) Profile plots of H3K4me3 CUT&Tag-normalized counts at TSSs ±2 kb of WT and *His^C* mutant embryos at 5.5 to 6 hours AEL separated by associated gene expression quartiles (q1 = lowest). Note the different scales for data with WT or *His^C* mutant embryos. (**B**) Representative snapshot of H3K4me3 CUT&Tag coverage tracks of WT (blue) and *His^C* mutant (green) embryos at 3.5 to 4, 4.5 to 5, and 5.5 to 6 hours AEL on chr 2L. Biological replicates are merged. (**C**) Profile plots of H3K4me3 CUT&Tag-normalized counts at called peaks (narrowPeak) ±2 kb of WT and *His^C* mutant embryos at 5.5 to 6 hours AEL. Blue denotes peaks called in WT only; green denotes peaks called in *His^C* mutant embryos only; gray denotes common (com.) peaks called in both genotypes.

peaks in intergenic regions shows enrichment in both genotypes, but their levels were different (Fig. 8, E and F, and fig. S17D). These results suggest that during replication in the absence of newly synthesized histones, H2A-H2B dimers harboring PTMs largely maintain their positional information.

DISCUSSION

Our data indicate that, in the absence of newly synthesized histones in a developing *Drosophila* embryo, parental nucleosomes are recycled and reassembled during DNA replication (Fig. 9). This finding is consistent with a previous study using *Xenopus* egg extracts, showing efficient recycling of parental histones upon depletion of the free histone pool (*32*). The resulting chromatin exhibits irregular nucleosomal arrays downstream of TSSs, which could be a consequence of reduced nucleosome occupancy and/or increased transcriptional activity (*33*), and also results in dispersal of active PTMs within gene bodies. Consistently, this results in spurious transcription, as was observed upon deletion of Chromodomain-Helicase DNA-binding 1 (CHD1) or Imitation Switch 1 (ISW1), which are chromatin remodelers with nucleosome spacing activity (*34*). In addition, the overall level of H3K36me3 across gene bodies is reduced, which was suggested to suppress spurious transcription (*35*). Despite these notable effects on the chromatin landscape, the genomic positions of histone modifications are not substantially altered during or after DNA replication, in particular, in intergenic regions. One explanation is that histone variants can partially compensate for histone demand, as shown for H3.3, a variant functionally redundant with H3 (*36*). Alternatively or in addition, nucleosomes of *His^C* mutants are at least partly reassembled as subnucleosomes including hexasomes or hemisomes, which is

apparent within gene bodies. Such subnucleosomes are wrapped by shorter stretches of DNA and are more fragile than nucleosomes (*17*), which supports our results showing reduced ATAC-seq fragment length distribution and nucleosome occupancy while maintaining the epigenetic landscape.

Our study reveals that, in a developing organism, such as the *Drosophila* embryo, active and repressive PTMs largely maintain their positional information during DNA replication, when parental nucleosomes provide the only available canonical histones. However, active marks become more dispersed, which is linked to active transcription. Notably, the levels of histone modifications become reduced at peaks, when new histones are not supplied during S phase. Moreover, our study establishes that parental histone H1 is recycled during DNA replication and that not only modified histone H3 but also modified H2A and H2B appear to exhibit a "positional memory" with respect to their previous location in the genome.

MATERIALS AND METHODS
Antibodies, oligonucleotides, fly stocks, software, and NGS libraries
Antibodies can be found in table S1. Oligonucleotides can be found in tables S2 to S4. Fly stocks can be found in table S5. Software used to analyze NGS data can be found in table S6. List of next-generation sequencing (NGS) libraries generated in this study including information on the number of independent biological replicates can be found in table S7.
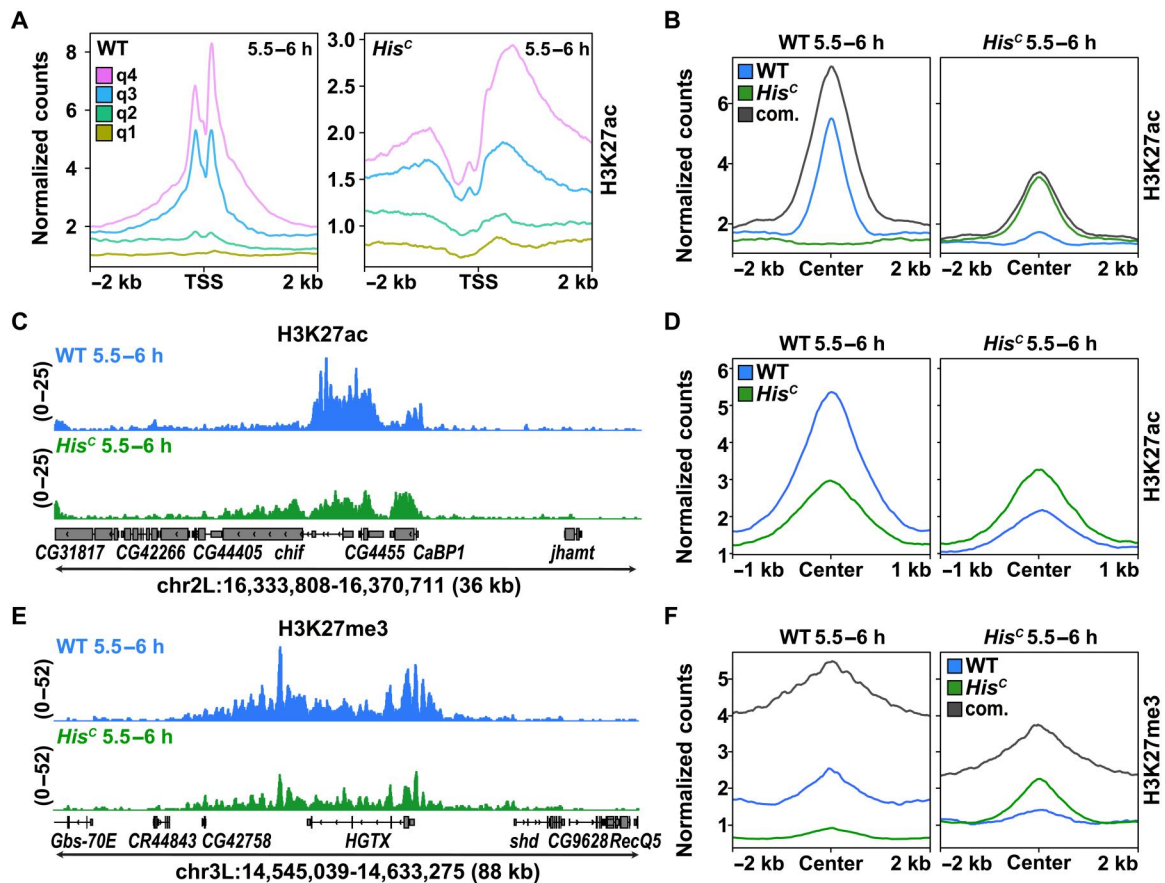
Fig. 7. Genomic positions of H3K27ac or H3K27me3 are largely preserved in *His^C* mutant embryos. (**A**) Profile plots of H3K27ac CUT&Tag-normalized counts at TSSs ±2 kb of WT and *His^C* mutant embryos at 5.5 to 6 hours AEL separated by associated gene expression quartiles (q1 = lowest). Note the different scales for data with WT or *His^C* mutant embryos. (**B**) Profile plots of H3K27ac CUT&Tag-normalized counts at called peaks (narrowPeak) of WT and *His^C* mutant embryos at 5.5 to 6 hours AEL. Blue denotes peaks called in WT only; green denotes peaks called in *His^C* mutant embryos only; gray denotes com. peaks called in both genotypes. (**C**) Representative snapshot of H3K27ac CUT&Tag coverage tracks of WT (blue) and *His^C* mutant (green) embryos at 5.5 to 6 hours AEL on chr 2L. Biological replicates are merged. (**D**) Profile plots of H3K27ac CUT&Tag-normalized counts at called peaks (narrowPeak) ±1 kb in intergenic regions of WT and *His^C* mutant embryos at 5.5 to 6 hours AEL. Blue denotes peaks called in WT; green denotes peaks called in *His^C* mutant embryos. (**E**) Representative snapshot of H3K27me3 CUT&Tag coverage tracks of WT (blue) and *His^C* mutant (green) embryos at 5.5 to 6 hours AEL on chr 2L. Biological replicates are merged. (**F**) Profile plots of H3K27me3 CUT&Tag-normalized counts at called peaks (broadPeak) of WT and *His^C* mutant embryos at 5.5 to 6 hours AEL. Blue denotes peaks called in WT only; green denotes peaks called in *His^C* mutant embryos only; gray denotes com. peaks called in both genotypes.

Fly strains and embryo collection

w^{1118} flies were used as wild-type controls. The generation of the *His^C* deletion, which covers the histone gene cluster on chromosome 2L, was described previously (*12*). To generate homozygous *His^C* mutant embryos, we crossed heterozygous *Df(2L)His^C, P{GAL4-twi.2xPE}/ CyO, P{ftz-lacB}E3* with *Df(2L)His^C, P{UAS:eYFP}AH2/ CyO, P{ftz-lacB}E3* flies. The resulting enhanced yellow fluorescent protein (eYFP)–expressing embryos with the genotype *Df(2L)His^C, P{GAL4-twi.2xPE}/ Df(2L)His^C, P{UAS:eYFP}AH2* were identified under a fluorescence stereomicroscope and collected with a P20 pipette. Nonfluorescent embryos from this cross with the genotypes *Df(2L)His^C, P{GAL4-twi.2xPE}/ CyO, P{ftz-lacB}E3, Df(2L)His^C, P{UAS:eYFP}AH2/ CyO, P{ftz-lacB}E3*, or *CyO, P{ftz-lacB}E3/ CyO, P{ftz-lacB}E3* were collected and used for H3K4me3 CUT&Tag shown in fig. S12B as an additional control. For time-staged embryo collections, flies were kept in cages covered by an apple agar plate at 25°C. Egg deposition on apple agar plates was restricted to 30 min, which were subsequently aged at 25°C for 3.5, 4.5, 5.5, or 6.5 hours.

Total RNA isolation

Embryos were dechorionated in 50% bleach and washed three times with phosphate-buffered saline (PBS) with 0.1% Tween 20 (PBS-T). Embryos were preserved in RNAlater (Invitrogen) and macerated in 50 µl of RLT buffer (QIAGEN RNeasy Plus Micro kit) using a precooled 1-ml Dounce homogenizer. The lysate was passed through a QIAshredder spin column (QIAGEN). RNA was then isolated using the QIAGEN RNeasy Plus Micro Kit. RNA concentration and quality were determined using a NanoDrop 2000 spectrometer (Thermo Fisher Scientific), Qubit 2.0 fluorometer (Invitrogen), and/or a 2200 TapeStation with High Sensitivity RNA screen tapes (Agilent).
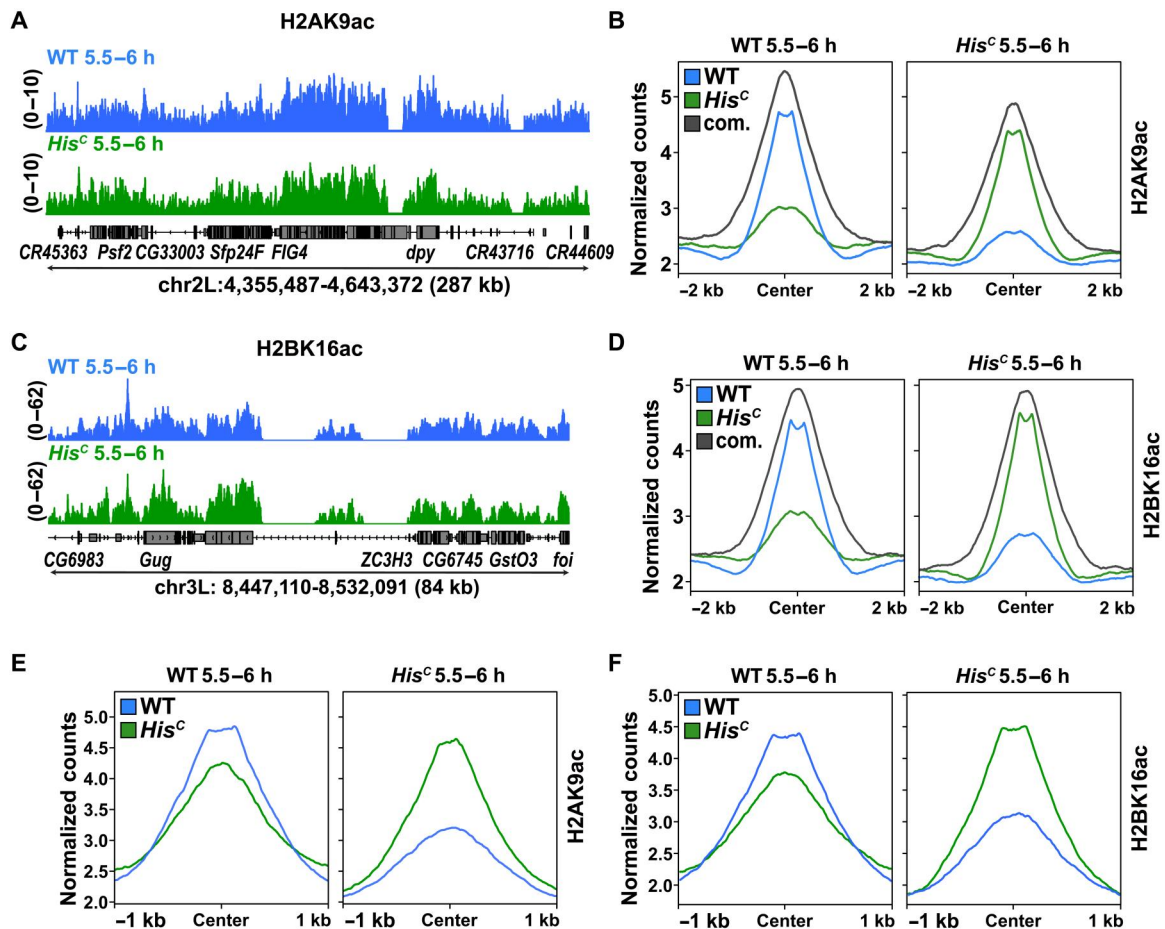
Fig. 8. Genomic positions of H2AK9ac or H2BK16ac are largely preserved in *His^C* mutant embryos. (**A**) Representative snapshot of H2AK9ac CUT&Tag coverage tracks of WT (blue) and *His^C* mutant (green) embryos at 5.5 to 6 hours AEL on chr 2L. Biological replicates are merged. (**B**) Profile plots of H2AK9ac CUT&Tag-normalized counts at called peaks (broadPeak) of WT and *His^C* mutant embryos at 5.5 to 6 hours AEL. Blue denotes peaks called in WT only; green denotes peaks called in *His^C* mutant embryos only; gray denotes com. peaks called in both genotypes. (**C**) Profile plots of H2AK9ac CUT&Tag-normalized counts at called peaks (broadPeak) ±1 kb in intergenic regions of WT and *His^C* mutant embryos at 5.5 to 6 hours AEL. Blue denotes peaks called in WT; green denotes peaks called in *His^C* mutant embryos. (**D**) Representative snapshot of H2BK16ac CUT&Tag coverage tracks of WT (blue) and *His^C* mutant (green) embryos at 5.5 to 6 hours AEL on chr 2L. Biological replicates are merged. (**E**) Profile plots of H2AK9ac CUT&Tag-normalized counts at called peaks (broadPeak) of WT and *His^C* mutant embryos at 5.5 to 6 hours AEL. Blue denotes peaks called in WT only; green denotes peaks called in *His^C* mutant embryos only; gray denotes com. peaks called in both genotypes. (**F**) Profile plots of H2BK16ac CUT&Tag-normalized counts at called peaks (broadPeak) ±1 kb in intergenic regions of WT and *His^C* mutant embryos at 5.5 to 6 hours AEL. Blue denotes peaks called in WT; green denotes peaks called in *His^C* mutant embryos.

Reverse transcription quantitative polymerase chain reaction

cDNA was amplified using the QuantiTect Reverse Transcription Kit (QIAGEN) with 50 ng of input RNA. Quantitative polymerase chain reaction (PCR) was performed using KAPA SYBR FAST Master Mix (2×) (Kapa Biosystems). Relative gene expression was analyzed using the comparative $\Delta\Delta Ct$ method using *Actin5C* for normalization (*37*).

RNA sequencing

Eighty nanograms of total RNA was used as input for each library preparation using Nugen Ovation *Drosophila* RNA-seq Systems 1-16 (0350-32). cDNA fragmentation was performed using a Covaris S2 (duty factor: 10%, cycle burst: 200, intensity: 5, and 210 s) sonicator. Libraries were amplified using 11 PCR cycles. Libraries were

multiplexed and sequenced using an Illumina HiSeq 4000 rapid run.

Assay for transposase-accessible chromatin using sequencing

ATAC-seq was performed as previously described with minor changes (*38, 39*). *His^C* mutant embryos arrest in G_2 phase of cell cycle 15 (*12*). To isolate ~50,000 nuclei, we collected 10 *His^C* mutant embryos for each experiment and developmental time point. To isolate a comparable number of nuclei from wild-type embryos, which proceed through cell cycle 15 and divide, we collected 10 embryos at 3.5 to 4 hours AEL, 8 embryos at 4.5 to 5 and 5.5 to 6 hours AEL, and 7 embryos at 6.5 to 7 hours AEL. Briefly, nuclei were isolated in 50 μl of lysis buffer [10 mM tris-HCl (pH 7.4), 10 mM NaCl, 3 mM MgCl, and 0.1% IGEPAL CA-630], and chromatin was tagmented in 45 μl of transposase mix
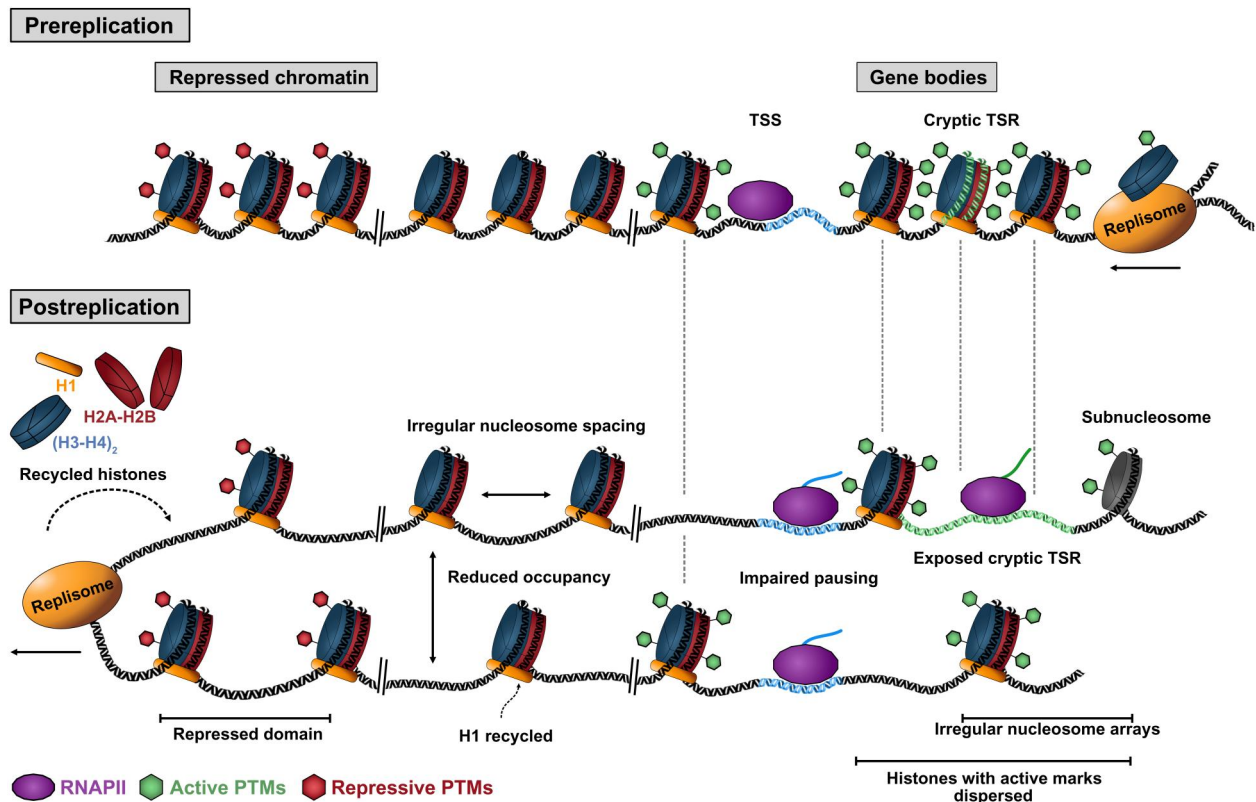
Fig. 9. Schematic representation of the chromatin landscape in *His*[C] mutant embryos. (Top) Chromatin prior replication. (**Bottom**) Chromatin after replication. RNAPII, RNA polymerase II.

(22.5 μl of Tagment DNA Enzyme 1 (TDE1) buffer, 23.75 μl of ddH$_2$O, and 1.25 μl of TDE1) for 75 min (Illumina TDE1 Tagment DNA Enzyme 15027865, TD buffer 15027866). Tagmented DNA was purified and subjected to PCR amplification using the following parameters: gap filling I at 58°C for 5 min, gap filling II at 72°C for 5 min, denaturation at 98°C for 30 s, 11× (denaturation at 98°C for 10 s, annealing at 63°C for 30 s, and extension at 72°C for 1 min), and final extension at 72°C for 3 min. Library was purified using 1.3× volume AMPure XP Beads (Beckman Coulter, A63881) and resuspended in 22 μl of 0.1× TE buffer. Libraries were multiplexed and sequenced (paired-end read 75) using a HiSeq 4000 (standard flow cell).

Cleavage under targets and tagmentation

CUT&Tag was performed as described previously with minor changes (*23*). Digitonin (Sigma-Aldrich, D141-100MG) was added to the final concentration of 0.05% to the respective buffers before use. Fifteen *His*[C] mutant and 12 wild-type embryos were collected for each experiment. Embryos were macerated using a 1-ml Dounce homogenizer with five to seven gentle strokes with a loose-fitting glass pestle in ice-cold PBS containing protease inhibitors (Roche, 4693132001). The cell lysate was centrifuged at 1200*g* for 5 min at 4°C. The supernatant was discarded, and the pellet was resuspended in ice-cold nuclear extraction buffer. The volume of concanavalin A (ConA) beads (Bangs Laboratories, BP531) per samples was adjusted to 5 μl. The nuclei were treated as described (*23*) and bound to the ConA beads. The beads were incubated in 50 μl of

antibody buffer containing 1× bovine serum albumin and 0.5 μg of primary antibody. Each sample was then incubated overnight at 4°C on an orbital shaker. The tubes were placed on a magnet, and the supernatant was discarded. Fifty microliters of secondary antibody solution (1:100 in digitonin wash buffer 150) was added and then incubated for 1 hour at room temperature. The beads were bound to a magnet and washed twice with digitonin wash buffer 150. One microliter of EpiCypher CUTANA pAG-TN5 (15-1017-EPC) mixed with 19 μl of digitonin wash buffer 300 was added to the beads and mixed by pipetting. After incubation at room temperature for 1 hour, the beads were separated on a magnet and washed twice with stringent digitonin wash buffer 300 without disturbing the beads. Tagmentation, stopping, and nuclei release was performed as described (*23*). For library amplification, 2× NEBNext HiFi PCR mix (M0541S) or 2× EpiCypher HiFi PCR mix (15-1018-EPC) was used. The following PCR program was used for all libraries: gap filling I at 58°C for 5 min, gap filling II at 72°C for 5 min, denaturation at 98°C for 30 s, 11× (denaturation at 98°C for 10 s and extension at 60°C for 10 s), and final extension at 72°C for 1 min. Libraries were purified using 0.9× volume of AMPure XP Beads (Beckman Coulter, A63881) and resuspended in 22 μl of 0.1× TE buffer. Libraries were multiplexed and sequenced (paired-end read 100) using a NovaSeq 6000 (SP or S1 flow cell).

Cleavage under targeted accessible chromatin

CUTAC was performed as described previously (*29*) using a rabbit anti-H3K4me2 antibody (Active Motif, 39142). The same

adjustments that were made for CUT&Tag were also applied for CUTAC. Tagmentation was performed by incubating the samples for 20 min at 37°C with CUTAC-hex tagmentation solution (5 mM MgCl$_2$, 10 mM TAPS, and 10% 1,6-hexanediol) in a thermocycler. Stopping, nuclei release, and library amplification as well as cleanup were performed as described for CUT&Tag. Libraries were multiplexed and sequenced (paired-end read 100) using a NovaSeq 6000 (SP flow cell).

Survey of transcription initiation at promoter elements with high-throughput sequencing

STRIPE-seq was performed as described previously (30). A total of 200 ng of total RNA was used as input for each replicate. TEX master mix (MP Biomedicals, 0210309705) was prepared by mixing 0.2 µl of terminator exonuclease (Lucigen, 162370) and 0.2 µl of terminator exonuclease reaction buffer A per sample. To digest uncapped or degraded mRNA, as well as ribosomal RNA, 1.6 µl or 200 ng of total RNA was incubated with 0.4 µl of TEX master mix and incubated for 1 hour at 30°C in a thermocycler. After incubation, the reverse transcription oligonucleotide was annealed by adding 1.5 µl of sorbitol/trehalose solution (DOT Scientific, DSS23080-500 and MP Biomedicals, 0210309705), 1 µl of RTO (10 µM), and 0.5 µl of deoxyribonucleotide triphosphates (dNTPs) (10 mM each) to each sample. The reactions were mixed by vortexing, spun down, and incubated first at 65°C for 5 min and then kept at 4°C for 2 min. For the template switching RT reaction, 2 µl of 5M betaine, 2 µl of 5× SuperScript IV reaction buffer (Invitrogen, 18090050B), 0.5 µl of 0.1 M dithiothreitol, and 0.5 µl of SuperScript IV reverse transcriptase (Invitrogen, 18090010) were mixed by vortexing and added to each RTO annealing reaction. The samples were incubated in a thermocycler at 25°C for 10 min, followed by 42°C for 5 min. Without removing the samples from the thermocycler, 0.25 µl of 400 µM template switching oligonucleotide was added, and the reactions were incubated subsequently for 25 min at 42°C followed by 10 min at 72°C. The samples were purified by adding 1.1× volume of AMPure XP beads (Beckman Coulter, A63881). After thorough mixing, the samples were incubated at room temperature for 10 min, followed by bead separation on a magnet. The beads were washed with 200 µl of 70% ethanol, air dried, and eluted in 20 µl of nuclease-free water after incubation at room temperature for 10 min. For library amplification 2.5 µl of forward library oligo and reverse library oligo were added together with 25 µl of 2× NEBNext ULTRAII Q5 HiFi PCR master mix. PCR was conducted with the following parameters: denaturation at 98°C for 3 min, 14× (denaturation at 98°C for 20 s, annealing at 60°C for 15 s, and extension at 72°C for 45 s), and final extension at 72°C for 2 min. Libraries were purified with double sided size exclusion using first 0.5× volume of AMPure XP beads and then increasing to 0.9× volume. Libraries were resuspended in 22 µl of 0.1× TE buffer. Libraries were multiplexed and sequenced (single-end read 100) using a NovaSeq 6000 (SP flow cell).

Western blots

All steps were performed on ice or at 4°C. Protein was isolated from 15 adult flies or 20 µl of wild-type or His^C mutant embryos by mechanical disruption in 200 µl of radioimmunoprecipitation assay buffer [50 mM tris-HCl, 150 mM NaCl, 1% NP-40, 0.5% sodium deoxycholate, 0.1% SDS, 1 mM EDTA, 10 mM NaF, 1 mM phenylmethylsulfonyl fluoride, 10 mM sodium butyrate, and protease inhibitors (Roche)], applying 10 strokes of a loose and subsequently of a tight-fitting pestle in a 200-µl Dounce homogenizer. DNA-bound proteins were released by sonication (7× 30-s on/off, medium intensity) using a Bioruptor Pico (Diagenode, B01060010). Debris was separated and discarded by centrifugation (15 min with 20,000g at 4°C). Protein concentration was measured using a Qubit 2.0 fluorometer (Invitrogen). After centrifugation, 4× loading buffer was added to the supernatant to a final concentration of 2×, and the samples were boiled for 5 min at 95°C. Twenty micrograms of protein per lane was separated using Bio-Rad Mini-PROTEAN TGX Precast 4 to 15% gradient gels using the Mini-PROTEAN Tetra Vertical Electrophoresis Cell (Bio-Rad) in 1× running buffer (25 mM tris-HCl, 190 mM glycine, and 0.1% SDS). Proteins were transferred onto a Immobilon-E polyvinylidene difluoride membrane (Merck Millipore, IEVH08100) applying 100 V for 60 min at 4°C in a wet transfer chamber (20 mM tris-HCl, 190 mM glycine, and 20% methanol). Membranes were washed in Tris-buffered saline with Tween20 (TBS-T) and blocked for 1 hour using 5% skim milk and subsequently incubated overnight at 4°C with the primary antibody [1:1000; α-RNAPIIS2P (Abcam, ab5095), α-RNAPII (Active Motif, 61668), α-H1 (Active Motif, 61786), α-H2AK9ac (Active motif, 39110), or α-H2BK16ac (Active Motif, 39122) in 5% skim milk]. Membranes were washed three times for 10 min in TBS-T and incubated with the secondary antibody [1:2000; horseradish peroxidase–conjugated α-Mm (SA00001-1, ProteinTech) or α-Rb (SA00001-2, ProteinTech) in 5% skim milk] for 2 hours at room temperature. Membranes were washed three times for 15 min in TBS-T, and the blots were developed using Pierce enhanced chemiluminescence (Thermo Fisher Scientific, 32109) and a ChemiDoc Imaging System (Bio-Rad).

RNA-seq data analysis

Quality check of the raw reads was done by FastQC v0.11.5 (www.bioinformatics.babraham.ac.uk/projects/fastqc) and subsequently mapped to the *D. melanogaster* reference genome assembly dm6 (FlyBase Dmel Release 6.23) using STAR v2.5.2b2 two-pass mode (40), with guidance from the gene models of FlyBase Dmel Release 6.23. Aligned reads were assigned to gene annotation using HTSeq-count version 0.10 (41). Differential gene expression was calculated using DESeq2 (42). Genes were considered differentially expressed between genotypes and time points if they had an absolute log$_2$fold change exceeding 1 and a P_{adj} of less than 0.01. PCA was performed by prcomp function and plotted by ggplot2 in R (43). Reads were normalized by scale factor using DESeq2 (42). Heatmaps were generated using the pheatmap R package (https://rdrr.io/cran/pheatmap/). Transcripts per kilobase million were calculated by RSEM v1.3.1 (44). GO enrichment analysis was performed using clusterProfiler (45).

ATAC-seq data analysis

Quality check of paired-end was done using FastQC v0.11.5 (www.bioinformatics.babraham.ac.uk/projects/fastqc). Nextera Transposase adapter and low-quality bases were eliminated using Trim Galore v0.6.6 (www.bioinformatics.babraham.ac.uk/projects/trim_galore) and Cutadapt v1.17 (46). After trimming, reads were mapped to the *D. melanogaster* reference genome dm6 (FlyBase Dmel Release 6.23) assembly using bowtie2 v2.3.4.2 (47). Mapped pairs were further filtered to maintain mapping quality above 10, as well as forward reverse (FR) orientation concordant alignments,

using custom scripts and samtools v1.9 (*48*). PCR duplicates and mitochondrial reads were removed by Sambamba v0.6.7 as well as reads blacklisted by the The Encyclopedia of DNA Elements (ENCODE) project (*49*, *50*). Peaks of accessible chromatin were identified for each sample using MACS2 v2.1.2 with the following settings: -f BED --nomodel --shift -100 --extsize 200 --keep-dup all after converting the BAM to BED file (*51*). Coverage tracks requiring bigwig files and heatmaps were generated using deepTools v3.3.1 (*52*). The nucleosome-free region and nucleosome positions were analyzed using NucleoATAC-0.3.4 (*16*). For Fig. 1 (C and D) and fig. S2 (E and F), paired-end reads were aligned to the Dmel R6.23 genome with Bowtie 2 (*47*) using --very-sensitive -X 2000 option. Low-quality [Mapping Quality (MAPQ)of <30] and mitochondrial reads were discarded. PCR duplicates were marked and removed using Picard (MarkDuplicates). Peaks were called using MACS2 with the −f BAMPE --keep-dup all options (*51*). For downstream analysis, we used peaks only present in at least two biological replicates. To identify inter-dyad distances around promoter regions, a window of ±2 kb around TSSs was used for nucleosome position extraction. Consistent peaks were annotated, and the nucleosome positions within intronic and intergenic regions in wild-types were extracted. These regions were used to define nucleosome positions within intronic and intergenic regions, respectively, for both wild-type and *His^C* mutant samples. PCA analysis was performed using ATAC-seq BAM files and DESeq2 (*42*).

CUT&Tag and CUTAC analysis

CUT&Tag and CUTAC datasets were processed as described for ATAC-seq. After read mapping using custom scripts and samtools v1.9 (*48*), peaks were called using MACS2 v2.1.2 (*51*) with the following settings: narrowPeak representation was used for histone marks H3K4me3, H2K27aC, and H3K4me2 with the following settings: -f BAMPE --keepdup all -p 5e-4 --call-summits. For histone marks enriched in broad domains including H3K36me3, H3K27me3, H2AK9ac, and H2BK16ac, the broadPeak representation was used applying the following settings: -f BAMPE --keepdup all -p 5e-4 -b 0.01. bigwig files required for coverage tracks and heatmaps were generated using deepTools v3.3.1 (*52*).

STRIPE-seq analysis

Quality of STRIPE-seq data sets was analyzed using FastQC v0.11.5 (www.bioinformatics.babraham.ac.uk/projects/fastqc). STRIPE-seq read files were processed and aligned to *D. melanogaster* reference genome dm6 (FlyBase Dmel Release 6.23) following the GoS-TRIPES workflow (https://github.com/BrendelGroup/GoSTRIPES) (*30*). Reads counts were further calculated, and TSSs were called using TSRchitect (https://bioconductor.org/packages/3.14/bioc/html/TSRchitect.html). The threshold for a TSS to be called was set to at least five raw counts that had to cluster into a TSR consistently in at least three of the analyzed replicates. Read counts were then normalized, and differential TSR analysis was performed using DESeq2 with default settings (*42*). TSR shape analysis was accomplished using TSRexploreR (*53*). Annotation of TSSs and TSRs was done with ChIPseeker using a promoter window from ±250 bp of a TSS (*54*). Genome browser tracks in bigwig format were generated from merged replicates using deepTools bamCoverage (*52*).

Figure preparation

Figures were assembled and labeled using Affinity Designer (https://affinity.serif.com). Coverage tracks were visualized using the Integrative Genomics Viewer (v2.12.3; https://igv.org).

Supplementary Materials

This PDF file includes:
Figs. S1 to S17
Tables S1 to S7

View/request a protocol for this paper from *Bio-protocol*.

REFERENCES AND NOTES

1. S. Ramachandran, S. Henikoff, Transcriptional regulators compete with nucleosomes post-replication. *Cell* **165**, 580–592 (2016).
2. K. R. Stewart-Morgan, N. Reverón-Gómez, A. Groth, Transcription restart establishes chromatin accessibility after DNA replication. *Mol. Cell* **75**, 284–297.e6 (2019).
3. N. Petryk, M. Dalby, A. Wenger, C. B. Stromme, A. Strandsby, R. Andersson, A. Groth, MCM2 promotes symmetric inheritance of modified histones during DNA replication. *Science* **361**, 1389–1392 (2018).
4. H. Gan, A. Serra-Cardona, X. Hua, H. Zhou, K. Labib, C. Yu, Z. Zhang, The Mcm2-Ctf4-Polα axis facilitates parental histone H3-H4 transfer to lagging strands. *Mol. Cell* **72**, 140–151.e3 (2018).
5. S. Mendiratta, A. Gatto, G. Almouzni, Histone supply: Multitiered regulation ensures chromatin dynamics throughout the cell cycle. *J. Cell Biol.* **218**, 39–54 (2019).
6. K. Ragunathan, G. Jih, D. Moazed, Epigenetic inheritance uncoupled from sequence-specific recruitment. *Science* **348**, 1258699 (2015).
7. P. N. C. B. Audergon, S. Catania, A. Kagansky, P. Tong, M. Shukla, A. L. Pidoux, R. C. Allshire, Restricted epigenetic inheritance of H3K9 methylation. *Science* **348**, 132–135 (2015).
8. K. R. Stewart-Morgan, N. Petryk, A. Groth, Chromatin replication and epigenetic cell memory. *Nat. Cell Biol.* **22**, 361–371 (2020).
9. G. Schlissel, J. Rine, The nucleosome core particle remembers its position through DNA replication and RNA transcription. *Proc. Natl. Acad. Sci. U.S.A.* **116**, 20605–20611 (2019).
10. N. Reverón-Gómez, C. González-Aguilera, K. R. Stewart-Morgan, N. Petryk, V. Flury, S. Graziano, J. V. Johansen, J. S. Jakobsen, C. Alabert, A. Groth, Accurate recycling of parental histones reproduces the histone modification landscape during DNA replication. *Mol. Cell* **72**, 239–249.e5 (2018).
11. T. M. Escobar, O. Oksuz, R. Saldaña-Meyer, N. Descostes, R. Bonasio, D. Reinberg, Active and repressed chromatin domains exhibit distinct nucleosome segregation during DNA replication. *Cell* **179**, 953–963.e11 (2019).
12. U. Günesdogan, H. Jäckle, A. Herzig, A genetic system to assess in vivo the functions of histones and histone modifications in higher eukaryotes. *EMBO Rep.* **11**, 772–776 (2010).
13. Y. Shindo, A. A. Amodeo, Dynamics of free and chromatin-bound histone H3 during early embryogenesis. *Curr. Biol.* **29**, 359–366.e4 (2019).
14. U. Günesdogan, H. Jäckle, A. Herzig, Histone supply regulates S phase timing and cell cycle progression. *eLife* **3**, e02443 (2014).
15. J. G. Henikoff, J. A. Belsky, K. Krassovsky, D. M. MacAlpine, S. Henikoff, Epigenome characterization at single base-pair resolution. *Proc. Natl. Acad. Sci. U.S.A.* **108**, 18318–18323 (2011).
16. A. N. Schep, J. D. Buenrostro, S. K. Denny, K. Schwartz, G. Sherlock, W. J. Greenleaf, Structured nucleosome fingerprints enable high-resolution mapping of chromatin architecture within regulatory regions. *Genome Res.* **25**, 1757–1770 (2015).
17. S. Ramachandran, K. Ahmad, S. Henikoff, Transcription and remodeling produce asymmetrically unwrapped nucleosomal intermediates. *Mol. Cell* **68**, 1038–1053.e4 (2017).
18. T. Kujirai, H. Kurumizaka, Transcription through the nucleosome. *Curr. Opin. Struct. Biol.* **61**, 42–49 (2020).
19. A. Bayona-Feliu, A. Casas-Lamesa, O. Reina, J. Bernués, F. Azorín, Linker histone H1 prevents R-loop accumulation and genome instability in heterochromatin. *Nat. Commun.* **8**, 283 (2017).
20. J. Hu, L. Gu, Y. Ye, M. Zheng, Z. Xu, J. Lin, Y. Du, M. Tian, L. Luo, B. Wang, X. Zhang, Z. Weng, C. Jiang, Dynamic placement of the linker histone H1 associated with nucleosome arrangement and gene transcription in early *Drosophila* embryonic development. *Cell Death Dis.* **9**, 765 (2018).
21. C. Alabert, J.-C. Bukowski-Wills, S.-B. Lee, G. Kustatscher, K. Nakamura, F. de Lima Alves, P. Menard, J. Mejlvang, J. Rappsilber, A. Groth, Nascent chromatin capture proteomics

determines chromatin dynamics during DNA replication and identifies unknown fork components. *Nat. Cell Biol.* **16**, 281–291 (2014).

22. Y. Isogai, S. Keles, M. Prestel, A. Hochheimer, R. Tjian, Transcription of histone gene cluster by differential core-promoter factors. *Genes Dev.* **21**, 2936–2949 (2007).

23. H. S. Kaya-Okur, S. J. Wu, C. A. Codomo, E. S. Pledger, T. D. Bryson, J. G. Henikoff, K. Ahmad, S. Henikoff, CUT&Tag for efficient epigenomic profiling of small samples and single cells. *Nat. Commun.* **10**, 1930 (2019).

24. J. Bednar, I. Garcia-Saez, R. Boopathi, A. R. Cutter, G. Papai, A. Reymer, S. H. Syed, I. N. Lone, O. Tonchev, C. Crucifix, H. Menoni, C. Papin, D. A. Skoufias, H. Kurumizaka, R. Lavery, A. Hamiche, J. J. Hayes, P. Schultz, D. Angelov, C. Petosa, S. Dimitrov, Structure and dynamics of a 197 bp nucleosome in complex with linker Histone H1. *Mol. Cell* **66**, 384–397.e8 (2017).

25. J. Wang, P. Rojas, J. Mao, M. Mustè Sadurnì, O. Garnier, S. Xiao, M. R. Higgs, P. Garcia, M. Saponaro, Persistence of RNA transcription during DNA replication delays duplication of transcription start sites until G2/M. *Cell Rep.* **34**, 108759 (2021).

26. The modENCODE Consortium, S. Roy, J. Ernst, P. V. Kharchenko, P. Kheradpour, N. Negre, M. L. Eaton, J. M. Landolin, C. A. Bristow, L. Ma, M. F. Lin, S. Washietl, B. I. Arshinoff, F. Ay, P. E. Meyer, N. Robine, N. L. Washington, L. D. Stefano, E. Berezikov, C. D. Brown, R. Candeias, J. W. Carlson, A. Carr, I. Jungreis, D. Marbach, R. Sealfon, M. Y. Tolstorukov, S. Will, A. A. Alekseyenko, C. Artieri, B. W. Booth, A. N. Brooks, Q. Dai, C. A. Davis, M. O. Duff, X. Feng, A. A. Gorchakov, T. Gu, J. G. Henikoff, P. Kapranov, R. Li, H. K. Mac Alpine, J. Malone, A. Minoda, J. Nordman, K. Okamura, M. Perry, S. K. Powell, N. C. Riddle, A. Sakai, A. Samsonova, J. E. Sandler, Y. B. Schwartz, N. Sher, R. Spokony, D. Sturgill, M. van Baren, K. H. Wan, L. Yang, C. Yu, E. Feingold, P. Good, M. Guyer, R. Lowdon, K. Ahmad, J. Andrews, B. Berger, S. E. Brenner, M. R. Brent, L. Cherbas, S. C. R. Elgin, T. R. Gingeras, R. Grossman, R. A. Hoskins, T. C. Kaufman, W. Kent, M. I. Kuroda, T. Orr-Weaver, N. Perrimon, V. Pirrotta, J. W. Posakony, B. Ren, S. Russell, P. Cherbas, B. R. Graveley, S. Lewis, G. Micklem, B. Oliver, P. J. Park, S. E. Celniker, S. Henikoff, G. H. Karpen, E. C. Lai, D. M. MacAlpine, L. D. Stein, K. P. White, M. Kellis, Identification of functional elements and regulatory circuits by *Drosophila* modENCODE. *Science* **330**, 1787–1797 (2010).

27. F. X. Chen, E. R. Smith, A. Shilatifard, Born to run: Control of transcription elongation by RNA polymerase II. *Nat. Rev. Mol. Cell Biol.* **19**, 464–478 (2018).

28. L. A. Gates, C. E. Foulds, B. W. O'Malley, Histone marks in the "drivers seat": Functional roles in steering the transcription cycle. *Trends Biochem. Sci.* **42**, 977–989 (2017).

29. S. Henikoff, J. G. Henikoff, H. S. Kaya-Okur, K. Ahmad, Efficient chromatin accessibility mapping in situ by nucleosome-tethered tagmentation. *eLife* **9**, e63274 (2020).

30. R. A. Policastro, R. T. Raborn, V. P. Brendel, G. E. Zentner, Simple and efficient profiling of transcription initiation and transcript levels with STRIPE-seq. *Genome Res.* **30**, 910–923 (2020).

31. M. P. Creyghton, A. W. Cheng, G. G. Welstead, T. Kooistra, B. W. Carey, E. J. Steine, J. Hanna, M. A. Lodato, G. M. Frampton, P. A. Sharp, L. A. Boyer, R. A. Young, R. Jaenisch, Histone H3K27ac separates active from poised enhancers and predicts developmental state. Proc. Natl. Acad. Sci. U.S.A. **107**, 21931–21936 (2010).

32. D. T. Gruszka, S. Xie, H. Kimura, H. Yardimci, Single-molecule imaging reveals control of parental histone recycling by free histones during DNA replication. *Sci. Adv.* **6**, eabc0330 (2020).

33. S. Baldi, S. Krebs, H. Blum, P. B. Becker, Genome-wide measurement of local nucleosome array regularity and spacing by nanopore sequencing. *Nat. Struct. Mol. Biol.* **25**, 894–901 (2018).

34. M. Smolle, S. Venkatesh, M. M. Gogol, H. Li, Y. Zhang, L. Florens, M. P. Washburn, J. L. Workman, Chromatin remodelers Isw1 and Chd1 maintain chromatin structure during transcription by preventing histone exchange. *Nat. Struct. Mol. Biol.* **19**, 884–892 (2012).

35. P. Sen, W. Dang, G. Donahue, J. Dai, J. Dorsey, X. Cao, W. Liu, K. Cao, R. Perry, J. Y. Lee, B. M. Wasko, D. T. Carr, C. He, B. Robison, J. Wagner, B. D. Gregory, M. Kaeberlein, B. K. Kennedy, J. D. Boeke, S. L. Berger, H3K36 methylation promotes longevity by enhancing transcriptional fidelity. *Genes Dev.* **29**, 1362–1376 (2015).

36. M. Hödl, K. Basler, Transcription in the absence of histone H3.2 and H3K4 methylation. *Curr. Biol.* **22**, 2253–2257 (2012).

37. T. D. Schmittgen, K. J. Livak, Analyzing real-time PCR data by the comparative C_T method. *Nat. Protoc.* **3**, 1101–1108 (2008).

38. J. D. Buenrostro, P. G. Giresi, L. C. Zaba, H. Y. Chang, W. J. Greenleaf, Transposition of native chromatin for fast and sensitive epigenomic profiling of open chromatin, DNA-binding proteins and nucleosome position. *Nat. Methods* **10**, 1213–1218 (2013).

39. J. D. Buenrostro, B. Wu, H. Y. Chang, W. J. Greenleaf, ATAC-seq: A method for assaying chromatin accessibility genome-wide. *Curr. Protoc. Mol. Biol.* **109**, 21.29.1–21.29.9 (2015).

40. A. Dobin, C. A. Davis, F. Schlesinger, J. Drenkow, C. Zaleski, S. Jha, P. Batut, M. Chaisson, T. R. Gingeras, STAR: Ultrafast universal RNA-seq aligner. *Bioinformatics* **29**, 15–21 (2013).

41. S. Anders, P. T. Pyl, W. Huber, HTSeq—A Python framework to work with high-throughput sequencing data. *Bioinformatics* **31**, 166–169 (2015).

42. M. I. Love, W. Huber, S. Anders, Moderated estimation of fold change and dispersion for RNA-seq data with DESeq2. *Genome Biol.* **15**, 550 (2014).

43. H. Wickham, *ggplot2: Elegant Graphics for Data Analysis* (Springer, ed. 1 2009; Corr. 3rd printing 2010 edition, 2010).

44. B. Li, C. N. Dewey, RSEM: Accurate transcript quantification from RNA-Seq data with or without a reference genome. *BMC Bioinformatics.* **12**, 323 (2011).

45. G. Yu, L.-G. Wang, Y. Han, Q.-Y. He, clusterProfiler: An R package for comparing biological themes among gene clusters. *OMICS* **16**, 284–287 (2012).

46. M. Martin, Cutadapt removes adapter sequences from high-throughput sequencing reads. *EMBnet J.* **17**, 10–12 (2011).

47. B. Langmead, S. L. Salzberg, Fast gapped-read alignment with Bowtie 2. *Nat. Methods* **9**, 357–359 (2012).

48. H. Li, B. Handsaker, A. Wysoker, T. Fennell, J. Ruan, N. Homer, G. Marth, G. Abecasis, R. Durbin, and 1000 Genome Project Data Processing Subgroup, The sequence alignment/map format and SAMtools. *Bioinformatics* **25**, 2078–2079 (2009).

49. A. Tarasov, A. J. Vilella, E. Cuppen, I. J. Nijman, P. Prins, Sambamba: Fast processing of NGS alignment formats. *Bioinformatics* **31**, 2032–2034 (2015).

50. H. M. Amemiya, A. Kundaje, A. P. Boyle, The ENCODE Blacklist: Identification of problematic regions of the genome. *Sci. Rep.* **9**, 9354 (2019).

51. Y. Zhang, T. Liu, C. A. Meyer, J. Eeckhoute, D. S. Johnson, B. E. Bernstein, C. Nusbaum, R. M. Myers, M. Brown, W. Li, X. S. Liu, Model-based analysis of ChIP-Seq (MACS). *Genome Biol.* **9**, R137 (2008).

52. F. Ramírez, F. Dündar, S. Diehl, B. A. Grüning, T. Manke, deepTools: A flexible platform for exploring deep-sequencing data. *Nucleic Acids Res.* **42**, W187–W191 (2014).

53. R. A. Policastro, D. J. McDonald, V. P. Brendel, G. E. Zentner, Flexible analysis of TSS mapping data and detection of TSS shifts with TSRexploreR. *NAR Genom. Bioinform.* **3**, lqab051 (2021).

54. G. Yu, L.-G. Wang, Q.-Y. He, ChIPseeker: An R/Bioconductor package for ChIP peak annotation, comparison and visualization. *Bioinformatics* **31**, 2382–2383 (2015).

Science Advances

Recycling of parental histones preserves the epigenetic landscape during embryonic development

Dominik Mhlen, Xiaojuan Li, Oleksandr Dovgusha, Herbert Jckle, and Ufuk Gnesdogan

View the article online
https://www.science.org/doi/10.1126/sciadv.add6440
Permissions
https://www.science.org/help/reprints-and-permissions

Use of this article is subject to the Terms of service